Structural performance and compression resistances of thin-walled square CFST columns with steel lining tubes

Xuhong Zhou[1], Jiepeng Liu[2], Xuanding Wang[3], Pengfei Liu[4], Kwok-Fai. Chung[5], Wei Wei[6]

Abstract: This paper proposes an innovative thin-walled square concrete-filled steel tubular (CFST) column with a circular/octagonal steel lining tube, in which the outer steel tube and the lining tube are fabricated independently of each other and then connected by slot welds. The advantages of a simplified manufacturing process, an insensitivity to local buckling, and a good confinement could be expected in this composite column. Twelve short columns were tested to failure under compression, and various key parameters including nominal width-to-thickness ratios of steel tubes, stiffener types, yield strengths of steel tubes and lining tubes were considered. The test results indicated that the proposed steel lining tubes were able to improve the axial behavior of these thin-walled square CFST short columns in various ways, including a more uniformly spaced buckling pattern with smaller intervals, larger axial stiffness, higher section resistances, and enhanced confinement and ductility. The octagonal lining tubes were more effective than the circular ones in terms of buckling constraints while the circular lining tubes were superior in terms of confining enhancement. A finite element parametric analysis was also carried out to assess the axial resistances of these thin-walled square CFST columns with lining tubes. A simplified model was developed incorporating both the post-local buckling of the square steel tubes and the confinement of the lining tubes.

Author keywords: Concrete-filled steel tubular column; Lining tube; Axial compression; Confinement; Numerical modeling.

[1]Professor, School of Civil Engineering, Chongqing University, Chongqing, 400045, China.

[2]Professor, School of Civil Engineering, Chongqing University, Chongqing, 400045, China.

[3]Ph.D., School of Civil Engineering, Chongqing University, Chongqing, 400045, China; Chinese National Engineering Research Centre for Steel Construction (Hong Kong Branch), Hong Kong Special Administrative Region (corresponding author). E-mail address: wangxuanding@cqu.edu.cn

[4]Master. Student, School of Civil Engineering, Chongqing University, Chongqing, 400045, China.

[5]Professor, Department of Civil and Environmental Engineering, The Hong Kong Polytechnic University, Hong Kong Special Administrative Region; Chinese National Engineering Research Centre for Steel Construction (Hong Kong Branch), Hong Kong Special Administrative Region.

[6]Associate Professor, School of Civil Engineering, Chongqing University, Chongqing, 400045, China.

1 Introduction

Concrete-filled steel tubular (CFST) columns have been increasingly popular in high-rise buildings, underground projects, and arch bridges due to the advantages of high section resistance, good ductility, and accelerated construction (Wei et al. 2020; Xiong et al. 2017; Han et al. 2014). However, in multi-story buildings, bridge piers, and other structures under relatively small axial loads, the use of CFST columns is not widespread due to increased construction costs comparing to those of conventional structures. One of the primary reasons is a large proportion of steel in these CFST structures. Current codes and specifications (AIJ 1997; AISC 2016; CEN 2004; MOHURD 2014) provide a maximum diameter/width-to-thickness ratio of steel tubes that prevents local buckling in the steel section under compression. Taking a square CFST column with Grade S355 steel as an example, the maximum width-to-thickness ratio of the steel tube is 42 according to EN1994-1-1 (CEN 2004). This indicates that the minimum steel-to-concrete area ratio of this CFST column that makes full use of the material strengths is about 9%, which is nearly 3 to 4 times that of a typical reinforced concrete column. Moreover, with an increase in the steel yield strength, the limitation of the maximum width-to-thickness ratio of the steel tubes in CFST columns will become more strict (Lee et al. 2016), which is unfavorable for promotion of effective use of high-strength steel in construction.

1.1 Thin-walled steel tubes with various stiffening schemes

Using thin-walled steel tubes in CFST structures is an effective way to improve the structural economy, including material saving, reduced welding workload, and simplified installation. Extensive experimental and theoretical investigations on thin-walled CFST columns have been conducted, and simplified models to predict their post-buckling resistances were proposed (Uy 2000; Liang et al. 2000). Despite the fact that local buckling does not significantly reduce the resistances of these thin-walled CFST columns owing to the advantageous confining effects on concrete (O'shea et al. 2000; Han et al. 2005), the potential ductility problem caused by premature buckling of the steel tubes under seismic loads is still a real concern to engineers, especially for the thin-walled square CFST columns which are susceptible to local buckling under limited confinement (Wu et al. 2012).

Various stiffening schemes have been proposed to postpone the local buckling, and hence, to improve the deformation characteristics of the thin-walled square CFST columns. Provision of longitudinal stiffeners to the inner surfaces of these square steel tubes is an effective way to enhance the longitudinal out-of-plane bending stiffness of the tube walls, and to divide them into multiple buckling zones in the transverse direction, thereby delaying the local buckling and changing the buckling patterns of these thin-walled square tubes. In addition, the composite effects between the steel tubes and the concrete are improved by the longitudinal stiffeners. Researchers (Ge et al. 1992; Tao et al. 2005; Huang et al. 2011; Petrus et al. 2010; Lee et al. 2019) have conducted a large number of axial compression tests to examine various key parameters including width-to-thickness of steel tubes, stiffness of stiffeners, and steel grades, etc. to verify the effectiveness of longitudinal stiffeners in improving the performance of these CFST columns. These test results indicated that the ductility of these thin-walled square CFST columns with longitudinal stiffeners should be further enhanced. Using transverse stiffeners or ties to restrict the out-of-plane buckling of the steel tubes and to improve confinement effects is another improvement scheme for these square CFST columns. Similar schemes include binding bars between opposite longitudinal stiffeners

(Tao et al. 2008; Dong et al. 2018), orthogonal/diagonal binding bars or ties (Huang et al. 2002; Yang et al. 2014; Wang et al. 2017), and diagonal binding ribs (Zhou et al. 2019).

1.2 Effectiveness of various stiffening schemes

Some existing test results of the thin-walled square CFST short columns under compression were collected to compare the effectiveness of different types of stiffeners, as shown in Fig. 1, where (1) only the specimens with width-to-thickness ratios of square tubes exceeding the limits specified in the Chinese Code GB 50936 (MOHURD 2014) ($[B/t]_{\max} = 60\sqrt{235/f_y}$) are included, (2) the average compressive strength of concrete is unified based on the conversion factors defined in the CEB-FIP Model Code (CEB-FIP 1993), and (3) SI and DI represent the strength index and the ductility index, respectively, and they are determined as follows:

$$\mathrm{SI} = \frac{N_u}{f_{y,t}A_t + f_{y,s}A_{s,e} + f_cA_c} \tag{1}$$

$$\mathrm{DI} = \frac{\varepsilon_{85\%}}{\varepsilon_y} \tag{2}$$

with B = width of cross-section, t = wall-thickness of square steel tube, N_u = experimental ultimate strength of the CFST columns, f_c = average compressive strength of concrete, $f_{y,t}$, $f_{y,s}$ = yield strengths of steel tube and stiffeners, respectively, A_c, A_t = cross-sectional areas of concrete core and steel tube, respectively, $A_{s,e}$ = equivalent cross-sectional area of stiffeners per unit height, $\varepsilon_{85\%}$ = axial strain when the load falls to 85% of the maximum load, ε_y = yield axial strain corresponding to the yield load determined by the geometric graphic method (Park 1988). Fig. 1 further highlights the importance of using stiffeners in these thin-walled square CFST columns in terms of material utilization efficiency and ductility improvement. The specimens with transverse stiffeners generally showed a more ductile behavior than those with longitudinal stiffeners. In a particular, the stiffening scheme by diagonal binding ribs (Zhou et al. 2019) shows superior effectiveness in improving both strength and ductility.

1.3 Proposed stiffening scheme using inner lining tubes

While provision of typical stiffeners in these thin-walled CFST short columns is important to achieve large section resistances under compression, these processes are often labor-intensive, and hence, expensive and time-consuming, leading to a significant decrease in the overall economy of these composite columns. Hence, an innovative stiffening scheme to thin-walled CFST columns is proposed by the authors in which inner lining tubes, in the forms of either circular or octagonal sections, are slot welded onto the outer steel tubes, as shown in Fig. 2. Potential benefits of the proposed stiffening scheme include:

a) the welding process for stiffening the outer steel tubes is significantly simplified,

b) the outer steel tubes are effectively restrained with the inner lining tubes so that their local buckling behavior is significantly enhanced, and

c) the structural behavior of these thin-walled CFST columns under compression is considerably improved owing to increased confinement to the concrete.

Thus, the proposed liner-stiffened steel tubes are expected to simplify the fabrication process as well as to improve the structural behavior of these thin-walled CFST columns considerably.

It is worthy to note that discontinuous slot welding allows the outer steel tube and the inner lining tube to be manufactured independently of each other, which simplifies the fabrication process and reduces the amount of welding materials. For example, the welding of the square steel tube with an octagonal lining tube is reduced by about 50~60% when compared with that of the same square steel tube with double longitudinal ribs. As a result, adverse effects of welding-induced residual stresses and defects on thin-walled steel tubes will be reduced considerably. Both the circular and the octagonal lining tubes, as closed hollow steel sections, can provide an effective enhancement in strength and confinement to the concrete core (Liu et al. 2018; Wang et al. 2015; Ding et al. 2016; Zhu et al. 2018).

Although the proposed steel lining tubes with slot welds are convenient and efficient for fabrication, only discontinuous point constraints are provided to the outer thin-walled square steel tubes. It is thus necessary to assess the post-local buckling performance of these liner-stiffened thin-walled CFST columns. Moreover, the confinement mechanism of the innovative composite sections is different from that of the conventional stiffened CFST columns. Thus, a complementary resistance model should be established.

1.4 Objectives and scope of work

This paper reports an experimental and numerical investigation into the structural behavior of the proposed liner-stiffened thin-walled CFST short columns under compression. The key test parameters are the stiffener types, the width-to-thickness ratios of the steel tubes, the yield strengths of the steel tubes. A finite element model is then established after a careful calibration against the test results while a good comparison between the measured and the predicted deformation characteristics of these columns is achieved. An extensive parametric analysis is carried out to provide sufficient numerical data for the development of a simplified resistance model incorporating both the post-local buckling behavior of the square steel tubes and the confinement of the steel lining tubes.

2 Experimental investigation

Twelve thin-walled square CFST short columns were tested to failure under compression. All the specimens are 720 mm in height and 240 mm in sectional width (height-to-width ratio = 3.0) with key parameters of the nominal width-to-thickness ratio of steel tube (B/t =120, 160), stiffener types (unstiffened, circular liner, and octagonal liner), yield strengths of steel tube/lining tube (271.9~424.7 N/mm^2). Details of the specimens are listed in Table 1, where H is the column height, t_l is the wall-thickness of the liner ($t_l = t$), A_t, A_l, A_c are respectively the cross-sectional areas of steel tube, liner, and concrete core, ρ is the steel ratio = $(A_t+A_l)/A_c$, and $[B/t]_{\mathrm{max}}$ and $[\rho]_{\mathrm{min}}$ are respectively the maximum width-to-thickness ratio of the square steel tube and the corresponding minimum steel-to-concrete area ratio which are determined by the Chinese Code GB 50936 (MOHURD 2014) for a square CFST column with the same steel grade with the test specimen — noted that the studied width-to-thickness ratios of the square steel tubes have significantly exceeded the code limits. The total steel ratios of the lined specimens were only 47~80%$[\rho]_{\mathrm{min}}$. For simplification, the unstiffened thin-walled square CFST specimens, the specimens with circular liners and those with octagonal liners are referred as “SU”, “SC”, and “SO”, respectively. The key parameters of the specimens are reflected in their nomenclature, where the initial abbreviation represents the specimen type, the number is the nominal width-to-thickness of the steel tube, and the last letter is used for labeling the specimens with the same parameters. For example, “120L” in Specimens SC-120L means that the width-to-thickness ratio of the steel tube is 120, and it is Grade S235 steel, which is lower than that of the other specimens (S355).

Fig. 3 shows the dimensions and configuration details of the SC and the SO specimens. All the square steel tubes, the circular liners, and the octagonal liners were fabricated by cold-forming thin-walled steel plates with only one longitudinal butt weld in each cell. The butt welds of the square and the octagonal steel tubes were respectively located at the corner of the square section and the middle of the sloping side of the octagonal section. The steel plates used for fabricating the square tubes of SC specimens and SO specimens were respectively pre-grooved with 4 and 8 columns of openings (30 mm long and 5 mm wide) according to the design drawing. The external sectional dimensions of the circular and the octagonal lining tubes are 2~4 mm smaller than the internal sectional sizes of the square tube for easy assembly. Both ends of the fabricated tubes were polished flatly to ensure that the lining tube has the same height as the square tube. A 16 mm thick enlarged endplate was welded at the bottom end of the square steel tube, then the circular or octagonal steel lining tube was placed into the square tube, and they were connected by the slot welding. The ready-mix concrete was cast into the lining tube and the sandwich cavity between the liner and the outer square steel tube. After the initial setting of concrete, high-strength cement was used for leveling the top surface, and then another endplate was welded to the top end of the square steel tube. Besides, the column ends were enhanced by end stiffeners. The SU specimens had a similar manufacturing process with the lined specimens except that no inner tube and slot holes were provided.

Tensile coupons were tested to determine the mechanical properties of the steel plates used in the specimens, as shown in Table 2 with f_y, f_u, E_s respectively representing the yield strength, the ultimate strength, and the elastic modulus of the steel plate. Sets of concrete cubes of 150 ×150 ×150 mm were prepared under the same condition as specimens and tested. Based on the average cubic strength ($f_{cu,150}$ = 44.7MPa), the average compressive strength of concrete used in the calculation is obtained according to the Model Code 1990 (CEB-FIP 1993) (f_c=36.5MPa).

Fig. 4 shows the testing machine and the instrumentations. All the specimens were tested under monotonically increasing compression using a hydraulic press, and the applied axial load was measured by a built-in load sensor. The specimen was placed directly on the machine's rigid plate and centered using a self-leveling cross-line laser. Four longitudinal linear variable displacement transducers (LVDTs) were mounted around the specimens to record the end-shortening. Several pairs of orthogonally arranged strain gauges were pasted on the external surface of the square steel tube at the column mid-height to monitor the longitudinal and transverse strains. Besides, the 2D GOM digital image correlation (DIC) technology (GOM 2015) was used to monitor the full-field displacement of the front surfaces where speckle patterns were sprayed.

2.1 Failure modes and observations

As shown in Fig. 5 and Fig. 6, the specimens failed in a combined manner of local buckling of steel tubes, rupture of welding or steel tubes, and crushing of concrete. The main damage characteristics are summarized in Table 3. The circular/octagonal lining tubes changed the failure mode of the thin-walled square CFST short columns in two aspects: (1) a more uniformly spaced buckling pattern with smaller spacings, and (2) more significant overall shear deformation of the concrete core.

Since the 2D DIC technology used in this test cannot capture the out-of-plane displacement of the steel tube, the longitudinal displacement field of the steel tube drawn by the DIC was employed to monitor the local buckling of the steel tube (Fig. 7). The initial buckling loads were estimated by the loads corresponding to the appearance of the first gray spot in the DIC pictures. In general, the lining tubes postponed the local buckling and almost doubled the buckling number on each side of the square steel tubes. Even though a few lined specimens even buckled earlier than the unstiffened ones due to initial imperfections or welding defects, this did not have a significant effect on both the buckling patterns and the axial behavior of these columns. For example, an initial buckling was observed in Specimen SC-160-a at a relatively small buckling load of $0.37N_u$. However, this premature buckling failed to develop into the main buckling and did not change the ultimate buckling pattern of this specimen (Fig. 5d). It could be concluded that the thin-walled square CFST columns with circular/octagonal lining tubes were not sensitive to initial imperfections or premature buckling. One of the reasons for this phenomenon is the stepwise buckling process of the lining specimens. As illustrated in Fig. 8, the buckling of the outer square steel tube will occur prior to that of the circular/octagonal liners and be restricted by the slot welding. As the load increases, more and more buckling waves appear, forming a multi-buckling pattern on the square steel tube. After the maximum loads, the circular and the octagonal lining tubes also undergo local buckling, which will reduce the confinement effect. This stepwise buckling mode would also help improve deformability and energy-dissipation ability of the composite column under seismic actions.

Rupture in the steel tube or the welding seam was another typical failure of the specimens, which was more likely to be observed in the lined CFST columns (6 specimens) rather than the unstiffened ones (1 specimen) due to the larger compressive strains and more severe buckling in the lined specimens (Fig. 6 and Table 3). Rupture in the steel tubes of the SC specimens was found mainly at the edges of the steel tubes with longitudinal welding seams while rupture in the SO specimens was common in the bent edges. Although initial rupture was mostly observed under the maximum loads, it did not cause a rapid drop in the section resistances of the lined specimens owing to the confinement of the circular or the octagonal lining tubes. Moreover, fracture in slot welding was seen only in two specimens at the unloading stage, indicating that the defects caused by slot welding had little influence on the compressive resistances. After the tests, the steel tubes were removed to observe the deformation of the concrete. For the SC and the SO specimens, the concrete between the square steel tubes and the lining tubes was found to be crushed and separated from the lining tubes.

2.2 Discussions on the main mechanical properties

Fig. 9 provides a comparison on the loads versus end-shortening curves of the specimens. It is found that the circular/octagonal lining tubes are able to improve the behavior of the thin-walled square CFST short columns under compression effectively, including larger axial stiffness, higher section resistance, prolonged elastoplastic stage, and a gradual load drop. Besides, the compressive resistances and the ductility of the specimens were also improved with the decreasing B/t ratios as well as the yield strengths of the steel tubes.

Table 4 shows the mechanical properties and performance indexes of the specimens, in which K is the tested axial stiffness of the specimen determined by the initial slope of the axial load (P) versus average axial strain (ε_l, and $\varepsilon_l = \delta/H$) curves, N_u and ε_u are respectively the maximum loads and peak average axial strain corresponding to N_u obtained from the test, K_0 is the nominal axial stiffness determined by Eq. (3), N_n is nominal resistance determined by Eq. (4), KI is the stiffness index of K to K_0 ratio, SI is the strength index of N_u to N_n ratio, and DI is the ductility index determined by Eq.(2). Moreover, the performance indexes of the two identical specimens are averaged and plotted as histograms in Fig. 10.

$$K_0 = \left(A_t + A_l\right) E_s + A_c E_c \tag{3}$$

$$N_n = \left(A_t + A_l\right) f_y + A_c f_c \tag{4}$$

According to Table 4 and Fig. 10, the mechanical properties in terms of axial stiffness, section resistance, and ductility are discussed as follows.

a) Axial stiffness

The axial stiffness of specimens with B/t = 120 and specimens with B/t = 160 was decreased by more than 5% and 20% with respect to the nominal axial stiffness, respectively. Provision of circular/octagonal lining tubes increased the initial stiffness due to the increase in the steel area, but it did not improve the stiffness index (KI) of these thin-walled CFST columns. Note that a significant difference (more than 30%) of axial stiffness between the two specimens with the same parameters was observed in certain groups, implying that the axial stiffness is sensitive to the initial imperfections of specimens and local buckling of the thin-walled steel tubes.

b) Section resistance

Although the B/t ratio of the steel tube is outside the limit of applicability recommended in the code, the two groups of unstiffened thin-walled CFST columns still reached their nominal resistance, which may be the results from the dual effects of the tube confinement and local buckling canceling each other out. Both the circular and the octagonal liners played a useful role in improving the axial resistances of thin-walled square CFST columns. The average resistance of Specimens SC-160 with a steel ratio of 4.5% was still 13% higher than the nominal resistance. Changing from the S355 steel to the S235 steel decreased the resistances of the specimens with circular liners by about 10%, but it had a moderate influence on SI.

c) Ductility

Significant improvement in axial deformability was gained for the lined CFST columns. The average peak axial strain of the specimens in group SC-120 was more than twice that of the specimens in group SU-120, and the ductility index of the former was nearly four times that of the latter. The ductility index of SC specimens decreased more than 50% with the wall-thickness of the square steel tube and the circular lining tube simultaneously reducing from 2.0mm to 1.5mm. Compared to the octagonal liners, the circular liners were more effective in improving ductility due to their enhanced confinement. Moreover, the scheme of circular/octagonal steel lining tubes in thin-wall square CFST columns has an advantage in term of ductility improvement, in comparison to the use of conventional longitudinal or transverse stiffeners (Fig. 1).

2.3 Strain analysis of steel tubes

Fig. 11 shows the relationship between the tube strains measured by the strain gauges (ε_{st} = transverse strain, ε_{sl} = longitudinal strain) and the average axial strain ε_l ($\varepsilon_l = \delta/H$) for typical specimens. The longitudinal tube strains showed an approximately synchronous increasing trend with the average axial strain in the initial elastic loading stage, with the ratio of ε_{st} to ε_{sl} being approximately the Poisson ratio. Since the strain gauges are used to monitor the strain development of the outer surfaces of the steel tubes at specific locations, the measured data is susceptible to factors such as initial defects and local buckling of the steel tubes. The occurrence of local buckling of the steel tubes at the measuring points is expected to affect the slopes of the strain curves, and the abrupt stiffness changing for the SU specimen is more significant than the liner-stiffened specimens. The steel lining tubes could generally increase both the longitudinal and the transverse strains of the square steel tubes at the peak loads. Compared to the strains measured in the middle of the sectional side, both the longitudinal and the transverse tube strains at the corners were fully developed, especially after the peak load. Therefore, the corners are the essential parts of the steel tubes for carrying the axial loads as far as confining the core concrete.

3. Finite element modeling

Finite element analyses using the ABAQUS software were carried out to simulate the behavior of the test specimens. The equivalent stress-strain relationship of concrete proposed by Han et al. (Han et al. 2007) was employed to determine the concrete properties in the finite element model. For the liner-stiffened specimens, the concrete model for the circular section is used with the following confinement factor,

$$\xi = \frac{A_l f_{y,l}}{A_c f_c} \tag{5}$$

The material properties of the steel tube in the finite element models were simplified as an elastic-perfectly plastic model. Other primary information of the finite element models includes: (1) The square steel tubes and the circular/octagonal lining tubes were modeled by the 4-nodes reduced integral shell element (S4R) with the simplified elastic perfectly-plastic material. (2) The concrete was modeled by the 8-nodes reduced integral solid element (C3D8R) with the material model of Concrete Damage Plasticity (CDP). (3) The plastic properties in the CDP model were taken as follows: Dilation Angle = 40, Eccentricity = 0.1, f_{b0}/f_{c0} = 1.16, K_c = 0.6667, Viscosity Parameter = 0.0001. (4) The mesh size of the model was taken as 20mm (1/12 of the sectional width). (5) The interaction between the square steel tube and the concrete was defined as Surface-to-Surface Contact, in which the normal behavior is defined as a Hard Contact allowing separation after the contact, and the tangential behavior is defined as Penalty Model with the friction coefficient taken as 0.6. (6) The slot welding was simulated by the Tie constraint technique. (7) The liner embedded into the concrete was constrained by the Embedded Region. (8) The endplates were simulated by two Rigid Body Constraints, which are respectively tied to the top surface and the bottom surface of the specimen, and the fixed boundary conditions were assigned to the Reference Points of the rigid surfaces. (9) The axial compression loads were applied to the reference point of the rigid top surface in the form of axial displacement.

3.1 Finite element results

As shown in Fig. 9, the finite element models are able to well predict the loads versus end-shorting curves of the specimens in terms of stiffness, section resistance, and ductility. The failure modes predicted by the finite element models are compared with the test results in Fig. 12, and a good agreement is apparent. To further verify the finite element model, the predicted axial resistances are examined by additional test data, as shown in Fig. 13. The mean of the predicted to the measured resistance ratios is 1.01, with a standard deviation of 0.04.

Based on the finite element models, the load-carrying mechanism and the stress distribution of the specimens were analyzed. The uniaxial stress contours of the steel tubes at the maximum loads are displayed in Fig. 14. The circular/octagonal lining tubes are effective to spread out the axial stresses uniformly in the thin-walled square steel tubes, and increase the resistance efficiency by constraining local buckling. By contrast, the octagonal lining scheme is superior to the circular one in term of buckling constraint. However, due to the discontinuous point-constrained mode of the slot-weld connections, it is still impossible to achieve an effective compression of the full-section of the thin-walled square steel tube. Fig. 15 shows the uniaxial stress contours of the concrete at the mid-height section corresponding to the maximum loads. Compared to the unstiffened specimen, the core concrete in the stiffened specimens is under effective confinement by the liners and bears increased uniaxial stresses. The circular liner provides more effective and uniform confinement to the concrete than that from the octagonal liner.

3.2 Parametric studies

Based on the finite element model, a systematic parametric study including 216 cases was carried out to assess the axial resistances of the thin-walled square CFST columns with lining tubes. The external dimensions of the studied cases are the same as the test specimens, and details of the parameter are listed in Table 5, where d_w is the longitudinal distance between the adjacent slot welding centers, and B_o is the side length of the octagonal liner parallel to the square steel tube. Fig. 16 illustrates the main results of the parametric study. The axial resistances of the calculated cases are found to be significantly influenced by the material strengths, the width to thickness ratios of the square steel tubes, and the thickness of the lining tubes. Enlarging the longitudinal distances of adjacent slot welds will slightly decrease the axial resistances of the SC cases, but this has little impact on the SO cases. Moreover, the axial resistances of the SO cases are almost the same when the side length of the octagonal liner (B_o) changed from 1/3(B-2t) to 1/2(B-2t).

4 Axial resistances of liner-stiffened thin-walled square CFST columns

Based on the test and the numerical results, the following simplifications are adopted to predict the axial resistances N_0 of the thin-walled square CFST columns with circular/octagonal lining tubes (Fig. 17).

a) The effective width model (Liang et al. 2000) is adopted to assess the post-buckling strength of the thin-walled square steel tube, in which any confining effect of the liners is ignored due to the discontinuous point-constrained mode of the slot-weld connections. The effective width (B_e) of the plates is determined as follows:

$$\frac{B_e}{B}=\begin{cases}0.675\left(\dfrac{\sigma_{cr}}{f_{y,t}}\right)^{1/3} & \sigma_{cr}\le f_y\\[2ex] 0.915\left(\dfrac{\sigma_{cr}}{\sigma_{cr}+f_{y,t}}\right)^{1/3} & \sigma_{cr}> f_y\end{cases} \tag{6}$$

$$\sigma_{cr}=\frac{10\pi^2E_s}{12\left(1-\mu_s^{\,2}\right)\left(B/t\right)^2} \tag{7}$$

where σ_{cr} is the critical stress, $f_{y,t}$ is the yield strength of the square steel tube, μ_s is the Poisson ratio of the steel tube.

b) The circular/octagonal lining tubes are assumed to carry no axial loads but to provide confinement to the concrete only. The effective confined area of concrete (Mander et al. 1988) is simplified to the area enclosed by the liners (Fig. 17). Therefore, the equivalent confining stress f_{el} may be calculated as follows,

$$f_{el} = k_e f_l \tag{8}$$

$$k_e = \frac{A_{c,e}}{A_c} \tag{9}$$

$$f_l = \begin{cases} 2t_s f_{y,l} / (B - 2t) & \text{SC specimen} \\ \sqrt{2} t_s 0.36 f_{y,l} / (B_{o1} - 2t) & \text{SO specimen} \end{cases} \tag{10}$$

where k_e is the ratio of the effective confined concrete area ($A_{c,e}$) to the entire concrete area (A_c), f_l is the confining stress of the circular liner or that of the octagonal liner, which is determined according to Wang et al. (2015) and Ding et al. (2016), respectively, $f_{y,l}$ is the yield strength of the liner, B_{o1} is the shorter edge length of the octagonal liner section.

Based on the simplifications, the axial resistance N_0 of the lined CFST columns is determined by,

$$N_0 = \frac{B_e}{B} A_t f_{y,t} + A_c f_{cc} \tag{11}$$

where f_{cc} is the confined concrete compressive strength estimated by the model proposed by Richart (for low lateral confinement < 7MPa) (Richart et al. 1928), and the increase in concrete strength by confinement was found to be 5.1 times the equivalent confining stress:

$$f_{cc} = f_c + 5.1 f_{el} \tag{12}$$

The axial resistances predicted by Eq. 11 are compared with the test results and those of the parametric study, as shown in Fig. 18. the simplified method makes good predictions to both the test and the numerical results. The average and the standard deviation of the ratios of N_0 calculated by Eq.11 to that predicted by the numerical model are found to be 0.97 and 0.03, respectively, demonstrating high accuracy of the proposed equations.

5 Conclusions

In this paper, an innovative thin-walled square CFST column with a circular/octagonal steel lining tube was proposed, and advantages of the proposed column include a simplified manufacturing process, an insensitivity to local buckling, and a good confinement. Twelve short columns were tested under compression, and their key parameters are the types of stiffeners, the width-to-thickness ratios of steel tubes, and the yield strengths of steel tubes. Finite element analyses were also carried out to assess the stress development and the axial resistances of the columns. The following conclusions were drawn.

(1) By providing circular/octagonal steel lining tubes, local buckling of thin-walled square CFST columns was postponed with a more uniformly spaced buckling pattern between smaller intervals. The lined specimens had a stepwise buckling mode that the external square steel tube buckled first then followed by the inner liner. This makes them insensitive to initial imperfections or premature buckling. Fracture of the longitudinal welds at the tube corners was observed in some specimens after mobilization of the peak loads, while the discontinuous slots were found to be relatively more robust due to the minimized welding defects.

(2) The circular/octagonal lining tubes improve the axial behavior of the thin-walled square CFST short columns effectively, including increased axial stiffness, larger section resistances, prolonged elastoplastic stage, and a gradual load drop. By

increasing the steel ratios by 2.0~2.6% (out of a total steel ratio at 4.5~5.9%), the axial resistances and the strength indexes of these lined specimens were approximately increased by 30% and 10%, respectively, compared with those of the unstiffened specimens, and the ductility indexes were increased by a factor of 1.6 to 3.9.

(3) The strength indexes of SC specimen were not influenced by the wall-thicknesses of the steel tubes in the scope of this study. However, the ductility index decreased more than 50% with the wall-thickness of the square steel tube and the circular liner simultaneously reducing from 2.0mm to 1.5mm. Changing the SC specimens from Grade S355 steel to Grade S235 steel could slightly decrease both the stiffness and the ductility indexes but this had a moderate influence on the strength index.

(4) The finite element results show that the inner liner improves the structural behavior of the thin-walled square CFST columns by restricting buckling of the square steel tube, and improving the confinement of the concrete. The octagonal lining tubes are more effective than the circular ones in term of buckling constraints, while the circular liners are superior in term of confining enhancement.

(5) An axial resistance model of the thin-walled square CFST column with a circular or octagonal steel lining tube was proposed after incorporating both the post-local buckling behavior of square steel tubes and the confinement of steel lining tubes. This model is shown to give axial resistances very close to both the measured and the predicted results.

It is worth noting that the conclusions drawn in this study and the proposed axial resistance model are readily applicable to the thin-walled CFST structures (B/t > 80). However, the liner-stiffened CFST columns with discontinuous slot weld proposed in this paper would also have a potential application in traditional thick-walled CFST columns, with advantages in reducing welding whilst enhancing confinement. Related research projects need to be further carried out.

DATA AVAILABILITY STATEMENT

Some or all data, models, or code that support the findings of this study are available from the corresponding author upon reasonable request.

ACKNOWLEDGMENTS

The authors are grateful to the supports provided by the National Natural Science Foundation of China (Grant No. 51890902 and 51908086), the China Postdoctoral Science Foundation (Project No. 2020T130758), and the Natural Science Foundation of Chongqing, China (Project No. cstc2019jcyj-bshX0091).

REFERENCES

AIJ (Architectural Institute of Japan). 1997. *Recommendations for design and construction of concrete filled steel tubular structures*. Tokyo: AIJ.

AISC (American Institute of Steel Construction). 2016. *Specification for structural steel buildings*. ANSI/AISC 360. Chicago: AISC.

CEB-FIP (Comité Euro-International du Béton/Federation Internationale de la Precontrainte). 1993. *CEB-FIP model code 1990 CEB bulletin d'Information*, Thomas Telford, London.

CEN (European Committee for Standardization). 2004. *Eurocode 4: Design of composite steel and concrete structures. Part 1.1: General rules and rules for building.* BS EN 1994-1-1. London: CEN.

Ding, F. X., Li, Z., Cheng, S., and Yu, Z. W. (2016). “Composite action of octagonal concrete-filled steel tubular stub columns under axial loading.” *Thin Wall Struct.*, 107, 453-461.

Dong, H., Li, Y., Cao, W., Qiao, Q., and Li, R. (2018). “Uniaxial compression performance of rectangular CFST columns with different internal construction characteristics.” *Eng. Struct.*, 176, 763-775.

Ge, H., and Usami, T. (1992). “Strength of concrete-filled thin-walled steel box columns: experiment.” *J. Struct. Eng.*, ASCE, 118(11), 3036-3054.

GOM (2015) Correlate Video Tutorial–2–Object Preparation and 2D Image Acquisition.

Han, L. H., Yao, G. H., and Zhao, X. L. (2005). Tests and calculations for hollow structural steel (HSS) stub columns filled with self-consolidating concrete (SCC). *J. Constr. Steel Res.*, 61(9), 1241-1269.

Han, L. H., Yao, G. H., and Tao, Z. (2007). “Performance of concrete-filled thin-walled steel tubes under pure torsion”. *Thin Wall Struct.*, 45(1), 24-36.

Han, L. H., Li, W., and Bjorhovde, R. (2014). “Developments and advanced applications of concrete-filled steel tubular (CFST) structures: Members.” *J. Constr. Steel Res.*, 100, 211-228.

Huang, C. S., Yeh, Y. K., Liu, G. Y., Hu, H. T., Tsai, K. C., Weng, Y. T., Wang, S. H., and Wu, M. H. (2002). “Axial load behavior of stiffened concrete-filled steel columns.” *J. Struct. Eng.*, ASCE, 128(9), 1222-1230.

Huang, H., Zhang, A., Li, Y., and Chen, M. (2011). “Experimental research and finite element analysis on mechanical performance of concrete-filled stiffened square steel tubular stub columns subjected to axial compression.” J. Build. Eng., 32(2), 75-82. (in Chinese)

Lee, H. J., Choi, I. R., and Park, H. G. (2016). “Eccentric compression strength of rectangular concrete-filled tubular columns using high-strength steel thin plates." *J. Struct. Eng.*, ASCE, 143(5), 04016228.

Lee, H. J., Park, H. G., and Choi, I. R. (2019). "Compression loading test for concrete-filled tubular columns with high-strength steel slender section." *J. Constr. Steel Res.*, 159, 507-520.

Liang, Q. Q., and Uy, B. (2000). "Theoretical study on the post-local buckling of steel plates in concrete-filled box columns." *Comput. Struct.*, 75(5), 479-490.

Liu, J., Teng, Y., Zhang, Y., Wang, X., and Chen, Y. F. (2018). "Axial stress-strain behavior of high-strength concrete confined by circular thin-walled steel tubes." *Constr. Build. Mater.,* 177, 366-377.

Mander, J. B., Priestley, M. J., and Park, R. (1988). "Theoretical stress-strain model for confined concrete". *J. Struct. Eng.*, ASCE, 114(8), 1804-1826.

MOHURD (Ministry of Housing and Urban-Rural Development of the People's Republic of China). 2014. *Technical code for concrete filled steel tubular structures.* [In Chinese.] GB50936. Beijing: MOHURD.

O'Shea, M. D., and Bridge, R. Q. (2000). Design of circular thin-walled concrete filled steel tubes. *J. Struct. Eng.*, ASCE, 126(11), 1295-1303.

Park R. (1988) "Ductility evaluation from laboratory and analytical testing." *Proc., 9th World Conference on Earthquake Engineering*, Tokyo-Kyoto, Japan, 8: 605-616.

Petrus, C., Hamid, H. A., Ibrahim, A., and Parke, G. (2010). "Experimental behaviour of concrete filled thin walled steel tubes with tab stiffeners." *J. Constr. Steel Res.*, 66(7), 915-922.

Richart, F. E., Brandtzaeg, A., and Brown, R. L. (1928). "A study of the failure of concrete under combined compressive stresses." University of Illinois at Urbana Champaign, College of Engineering, Engineering Experiment Station.

Tao, Z., Han, L. H., and Wang, Z. B. (2005). “Experimental behaviour of stiffened concrete-filled thin-walled hollow steel structural (HSS) stub columns.” *J. Constr. Steel Res.*, 61(7), 962-983.

Tao, Z., Han, L. H., and Wang, D. Y. (2008). “Strength and ductility of stiffened thin-walled hollow steel structural stub columns filled with concrete.” *Thin Wall Struct.*, 46(10), 1113-1128.

Uy, B. (2000). “Strength of concrete filled steel box columns incorporating local buckling.” *J. Struct. Eng*, ASCE, 126(3), 341-352.

Wang, X., Liu, J., and Zhang, S. (2015). “Behavior of short circular tubed-reinforced-concrete columns subjected to eccentric compression.” *Eng. Struct.*, 105, 77-86.

Wang, Y. T., Cai, J., and Long, Y. L. (2017). “Hysteretic behavior of square CFT columns with binding bars.” *J. Constr. Steel Res.*, 131, 162-175.

Wei, J., Luo, X., Lai, Z., and Varma, A. H. (2020). “Experimental Behavior and Design of High-Strength Circular Concrete-Filled Steel Tube Short Columns.” *J. Struct. Eng.*, ASCE, 146(1), 04019184.

Wu, B., Zhao, X. Y., and Zhang, J. S. (2012). “Cyclic behavior of thin-walled square steel tubular columns filled with demolished concrete lumps and fresh concrete.” *J. Constr. Steel Res.*, 77, 69-81.

Xiong M., Xiong D., Liew J. (2017). “Behaviour of steel tubular members infilled with ultra high strength concrete.” *J. Constr. Steel Res.*, 138, 168-183.

Yang, Y., Wang, Y., and Fu, F. (2014). “Effect of reinforcement stiffeners on square concrete-filled steel tubular columns subjected to axial compressive load.” *Thin Wall Struct.*, 82, 132-144.

Zhou, Z., Gan, D., and Zhou, X. (2019). “Improved composite effect of square concrete-filled steel tubes with diagonal binding ribs.” *J. Struct. Eng.*, 145(10), 04019112.

Zhu, J. Y., and Chan, T. M. (2018). “Experimental investigation on octagonal concrete filled steel stub columns under uniaxial compression.” *J. Constr. Steel Res.*, 147, 457-467.

List of Tables:

Table 1. Specimen details

No.	Specimen	H (mm)	B (mm)	t (mm)	B/t	$[B/t]_{max}$	Liner type	t_l (mm)	A_t (mm^2)	A_l (mm^2)	A_c (mm^2)	ρ (%)	$[\rho]_{min}$ (%)
1	SU-120-a	720	240	1.89	120	47	/	1.89	1800	0	55800	3.2	9.2
2	SU-120-b	720	240	1.89	120	47	/	1.89	1800	0	55800	3.2	9.2
3	SU-160-a	720	240	1.46	160	45	/	1.46	1393	0	56207	2.5	9.6
4	SU-160-b	720	240	1.46	160	45	/	1.46	1393	0	56207	2.5	9.6
5	SC-120-a	720	240	1.89	120	47	Circular	1.89	1800	1391	54409	5.9	9.2
6	SC-120-b	720	240	1.89	120	47	Circular	1.89	1800	1391	54409	5.9	9.2
7	SC-120L-a	720	240	1.97	120	56	Circular	1.97	1876	1449	54276	6.1	7.6
8	SC-120L-b	720	240	1.97	120	56	Circular	1.97	1876	1449	54276	6.1	7.6
9	SC-160-a	720	240	1.46	160	45	Circular	1.46	1393	1081	55126	4.5	9.6
10	SC-160-b	720	240	1.46	160	45	Circular	1.46	1393	1081	55126	4.5	9.6
11	SO-120-a	720	240	1.89	120	47	Octagonal	1.89	1800	1460	54340	6.0	9.2
12	SO-120-b	720	240	1.89	120	47	Octagonal	1.89	1800	1460	54340	6.0	9.2

Table 2. Properties of the steel plate

Steel grade	t (mm)	f_y (MPa)	f_u (MPa)	E_s (GPa)
S355	1.46	424.7	556.1	216
S355	1.89	389.0	520.7	174
S235	1.97	271.9	361.4	167

Table 3. Damage characteristics

Specimen	Buckling loads	Buckling number in each side-face n_b	Fracture position	Fracture loads
SU-120-a	0.77 N_u	1~2	/	/
SU-120-b	0.58 N_u	2~3	Longitudinal weld	N_u
SU-160-a	0.69 N_u	2~3	/	/
SU-160-b	0.76 N_u	2~3	/	/
SC-120-a	0.87 N_u	3~5	Longitudinal & slot weld	N_u
SC-120-b	0.81 N_u	4~5	Longitudinal & slot weld	$0.85N_u^*$
SC-120L-a	0.81 N_u	4~5	/	/
SC-120L-b	0.91 N_u	3~5	Longitudinal weld	N_u
SC-160-a	0.37 N_u	3~6	Longitudinal weld	$0.85N_u^*$
SC-160-b	0.65 N_u	4~5	/	/
SO-120-a	0.85 N_u	3~6	Tube edge with no weld	N_u
SO-120-b	0.94 N_u	3~5	Tube edge with no weld	N_u

*Note: $0.85N_u^*$ means that the axial bearing capacity drops to 85% of the maximum loads.

Table 4. Mechanical properties

Specimen	ρ (%)	K (10^6kN)		K_0 (10^6kN)	KI	N_u (kN)		N_0 (kN)	SI	ε_u (10^{-6})		DI	
		/	AVG			/	AVG			/	AVG	/	AVG
SU-120-a	3.2	1.88	1.82	1.91	0.95	2855.4	2891.6	2736.9	1.06	2799	3003	1.93	1.95
SU-120-b	3.2	1.75				2927.7				3206		1.96	
SU-160-a	2.5	1.20	1.50	1.91	0.79	2809.0	2716.5	2643.2	1.03	3742	3282	1.69	2.15
SU-160-b	2.5	1.81				2624.0				2821		2.60	
SC-120-a	5.9	2.28	2.02	2.11	0.96	3763.8	3734.5	3227.2	1.16	6619	6849	8.21	7.53
SC-120-b	5.9	1.76				3705.2				7078		6.85	
SC-120L-a	6.1	1.89	1.88	2.11	0.89	3294.4	3307.3	2885.1	1.15	6534	5614	5.82	5.60
SC-120L-b	6.1	1.88				3320.1				4693		5.38	
SC-160-a	4.5	1.46	1.55	2.11	0.73	3540.4	3467.7	3062.8	1.13	6457	5266	3.54	3.49
SC-160-b	4.5	1.63				3395.0				4075		3.44	
SO-120-a	6.0	1.47	1.85	2.12	0.87	3795.4	3798.7	3251.6	1.17	5052	4545	4.25	5.70
SO-120-b	6.0	2.22				3802.0				4037		7.15	

Table 5. Parameter details

Parameters	Values
B/t	80, 110, 140
t_l/t	0.8, 1.0, 1.2
d_w/B	0.3, 0.5
$B_o/(B-2t)$ (SO specimens)	1/3, 1/2
f_y (MPa)	235, 420
f_c (MPa)	25, 40

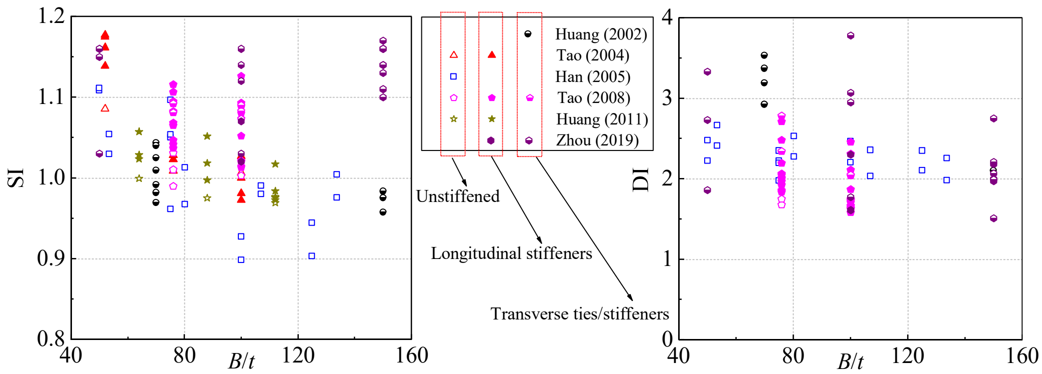

Fig. 1. Comparison of strength and ductility indexes for columns with different stiffeners

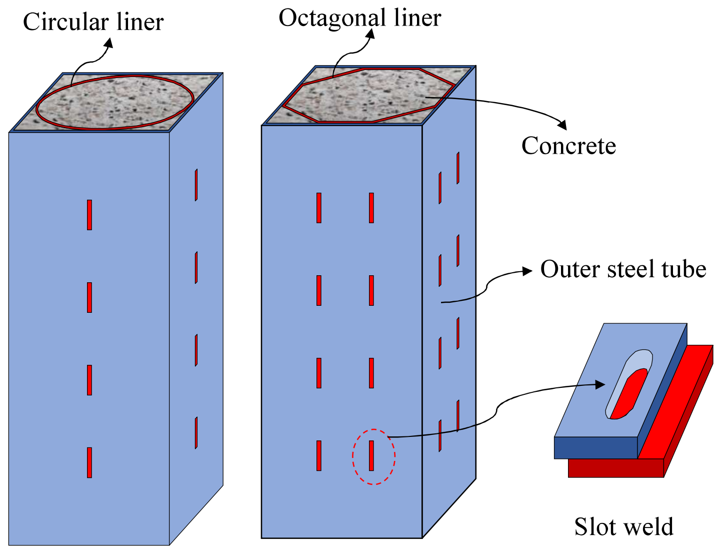

Fig. 2. Illustration of the square CFST with circular/octagonal liner

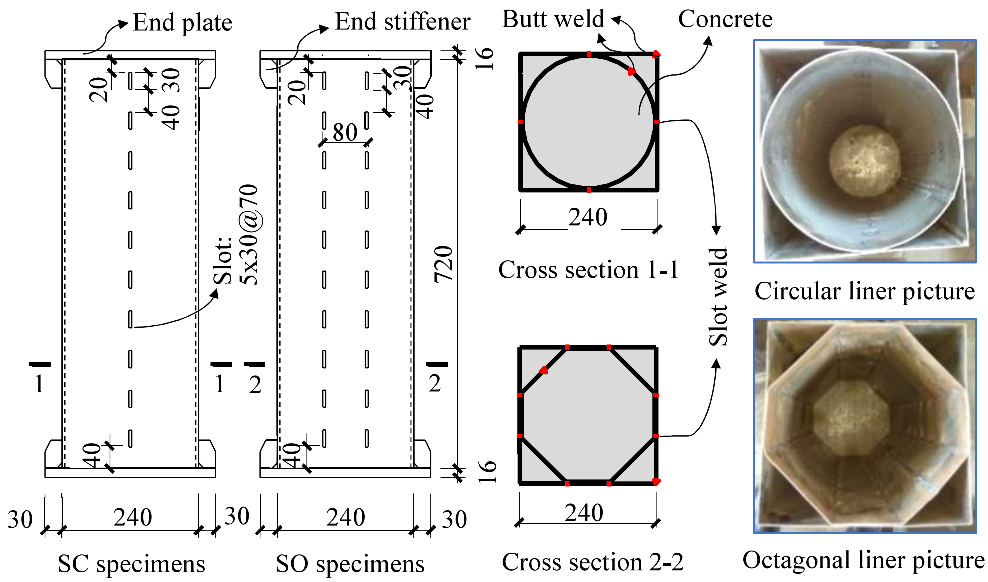

Fig. 3. Dimensions and configuration details of the SC and SO specimens (unit: mm)

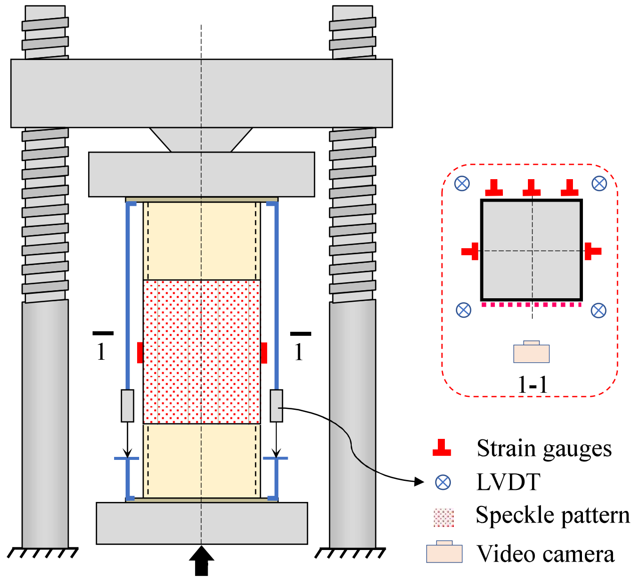

Fig. 4. Testing machine and instrumentations

(a) SU-120-b (b) SU-160-b (c) SC-120-b (d) SC-160-a (e) SO-120-a

Fig. 5. Failure modes of typical specimens

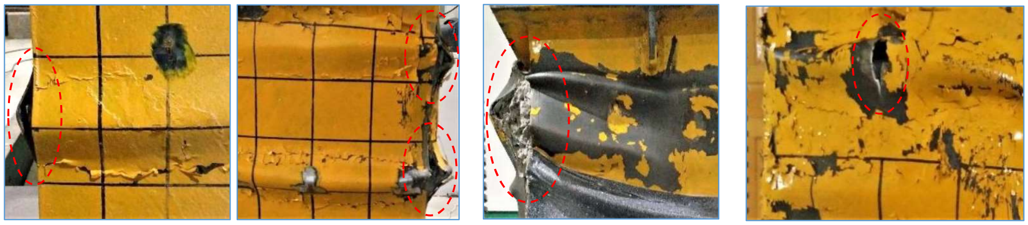

(a) Longitudinal weld (b) Tube corner (c) Slot weld

Fig. 6. Rupture in steel tube

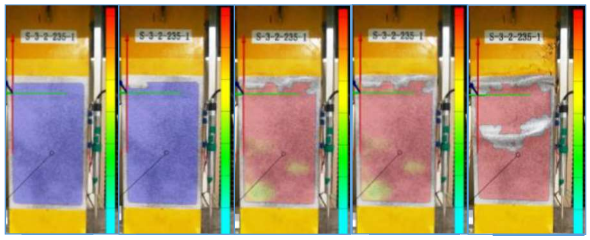

$0.50N_u$ $0.85N_u$ N_u $0.85N_u^*$ $0.70N_u^*$

Fig. 7. DIC displacement field of steel tube

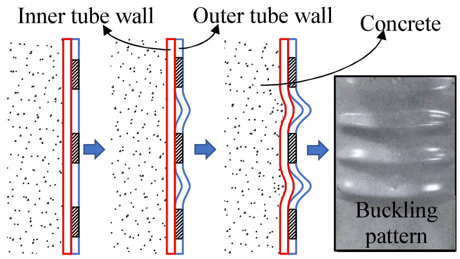

Fig. 8. Stepwise buckling mode

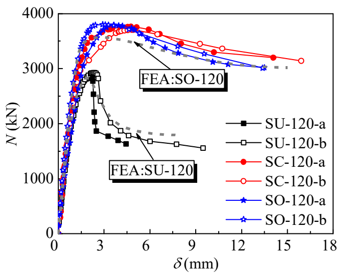

(a) Group1

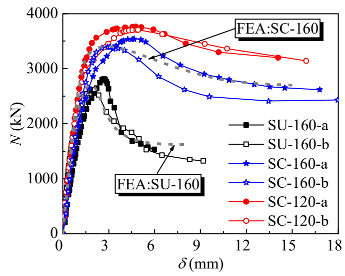

(b) Group2

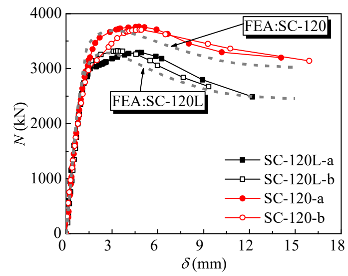

(c) Group3

Fig. 9. Loads versus end-shortening curves

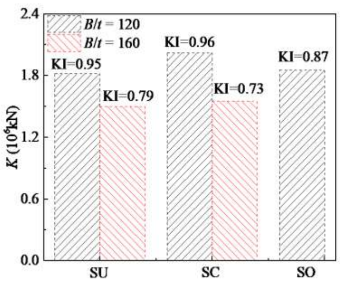

(1) Axial stiffness

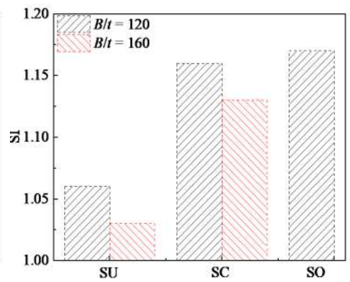

(2) Strength index

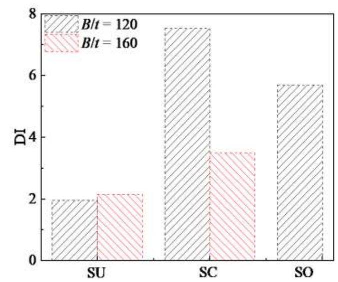

(3) Ductility index

Fig. 10. Comparison of performance indexes

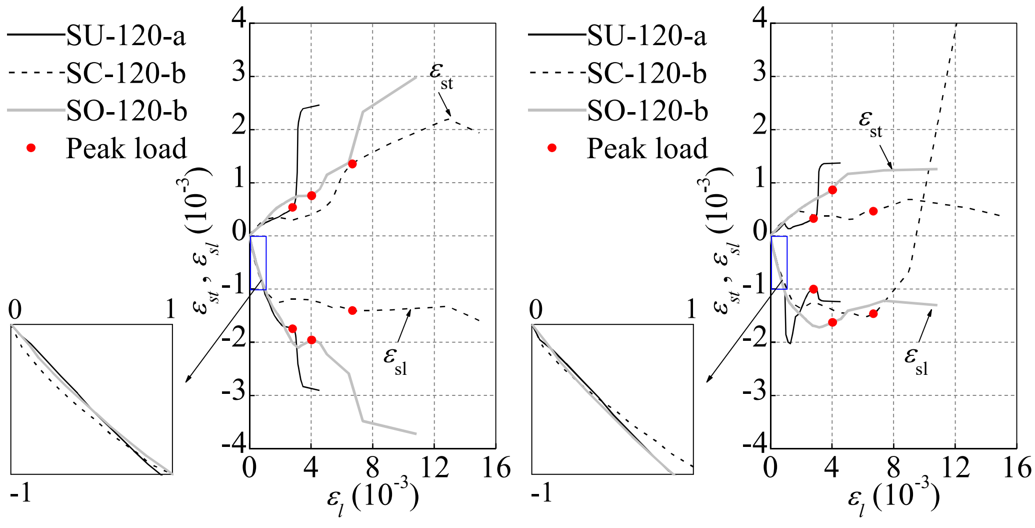

(a) Strains at the sectional corners (b) Strains in the middle of the sectional sides

Fig. 11 Typical curves of the measured tube strain versus the average axial strain

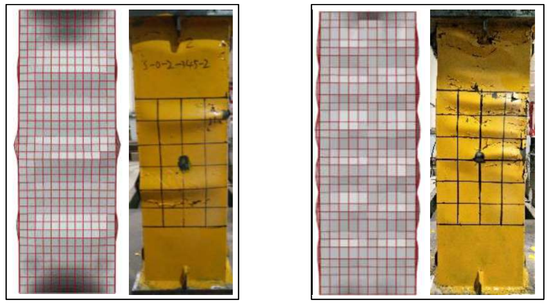

(a) SU specimen (b) SC specimen

Fig. 12. Failure mode comparison

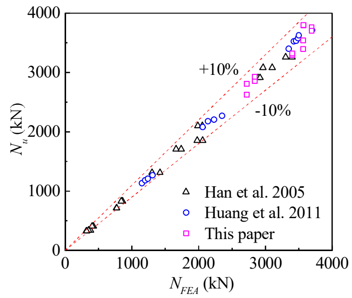

Fig.13. Verification of FE models

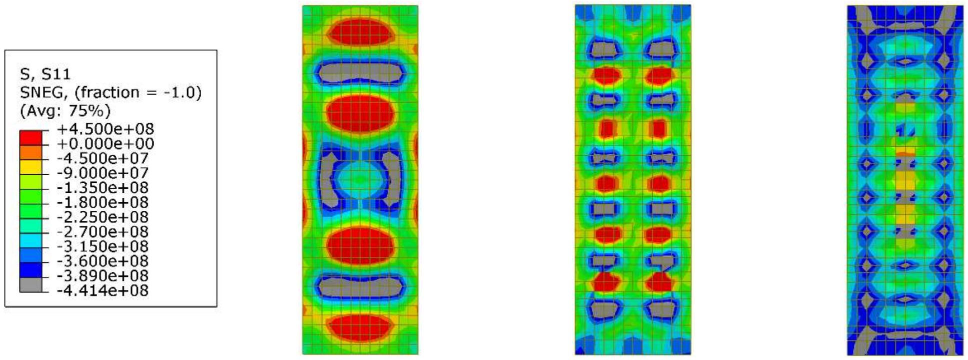

(a) Legend (N/m^2) (b) SU specimen (b) SC specimen (c) SO specimen

Fig. 14. Uniaxial stress contours of steel tube

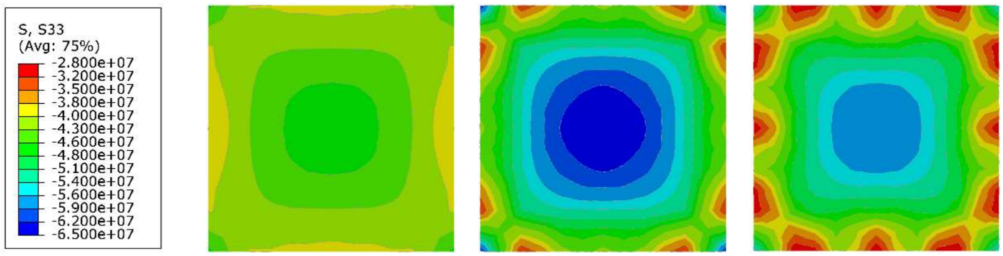

(a) Legend (N/m^2) (b) SU specimen (b) SC specimen (c) SO specimen

Fig. 15. Uniaxial stress contours of concrete at mid-height section

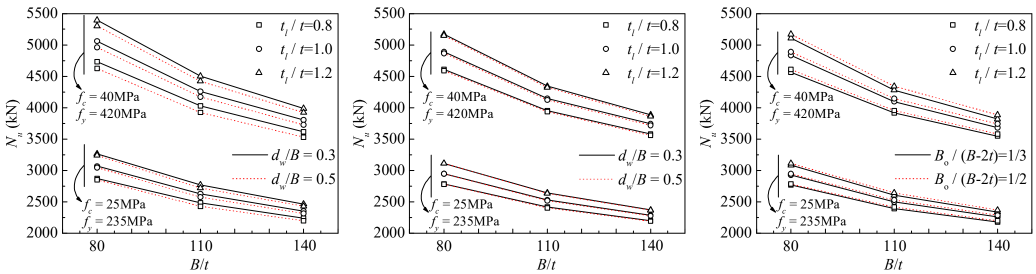

(a) SC cases (b) SO cases ($B_o/(B\text{-}2t)$ = 1/2) (c) SO cases (d_w/B = 0.3)

Fig. 16. Parametric analysis

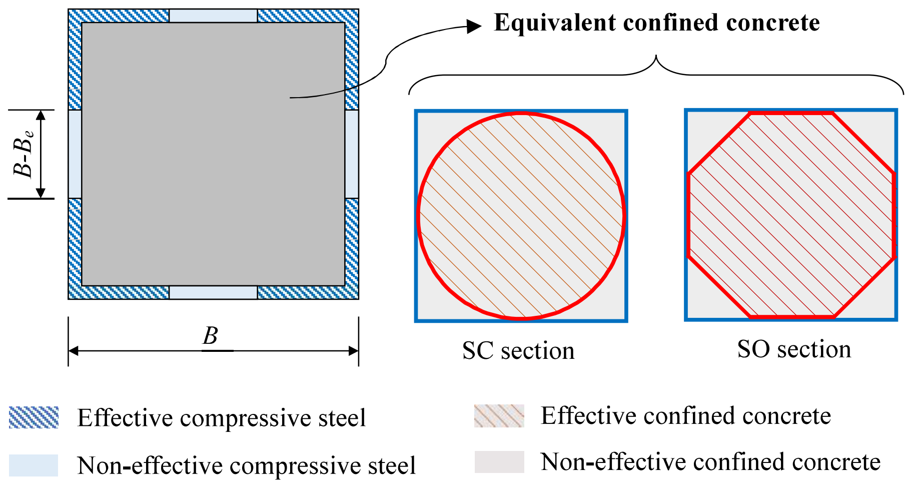

Fig. 17. Illustration of the simplified axial resistance model for the lined columns

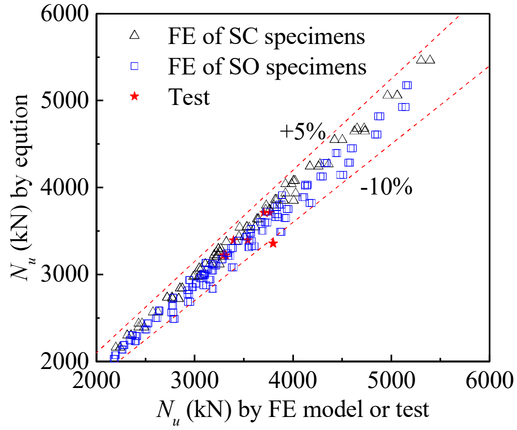

Fig. 18. Verification of the proposed resistance model